RSC Advances

ROYAL SOCIETY OF CHEMISTRY

www.rsc.org/advances

Journal Name

ARTICLE

Received 00th January 20xx,
Accepted 00th January 20xx
DOI: 10.1039/x0xx00000x
www.rsc.org/

Band Gap and Schottky Barrier Engineered Photocatalyst with Promising Solar Light Activity for Water Remediation

V. Jabbari [a], M. Hamadanian [b,c*], M. Shamshiri [c], D. Villagrán [a]

Abstract

Novel nanophotocatalyst of Mo- and S-doped TiO_2 (Mo,S-codoped TiO_2) was synthesized via a modified sol–gel in conjunction with photochemical reduction. The XRD results showed all of the prepared nanocatalysts contain only anatase phase. The SEM and TEM analyses revealed the doping of Mo and S does not leave any change in morphology of the TiO_2 catalyst. Chemical composition analysis carried out with EDX confirmed successful doping of TiO_2 by Mo and S elements and DRS illustrated band gap reduction in TiO_2 after the doping. The photocatalytic performance of the samples was tested on degradation of methyl orange (MO) as model organic pollutant. The results showed photocatalytic activity of the Mo(0.06%), S(0.05%)-codoped TiO_2 catalyst was higher than that of other catalysts under UV and visible light irradiation. Indeed, due to the synergetic effect of doping of S and Mo, Mo,S-codoped TiO_2 catalyst has higher photoactivity than the sole TiO_2 and TiO_2 doped solely with either Mo or S. Finally, it is proposed that that the newly developed Mo,S-codoped TiO_2 Photocatalyst can be a great candidate for environmental applications such as air and water purification.

Keywords: Mo,S-doped TiO_2; Band Gap Engineering, Photo-Catalyst, Visible light

1. Introduction

Due to resistance to photocorrosion, good physical and chemical stability, low cost, non-toxicity and strong oxidizing power, TiO_2 is the most widely used photocatalyst in photodegradation of organic pollutants for air and water purifications [1-5]. However, TiO_2 has a relatively large band gap (3.20 eV for anatase TiO_2) which enables it to absorb only UV portion of solar light (~5%). Many techniques have been examined for extension of the light absorption threshold of TiO_2 to visible light and near-IR region of solar light such as dye sensitization [6], transition metals doping [7], noble metal deposition [8], and anion doping [9,10].

Lately, doping of non-metal elements into TiO_2 photocatalyst become a hot research topic, which opens up a new possibility for the development of solar- or visible light-active photocatalytic materials. Doping of non-metal ions into TiO_2 can shift its optical absorption edge from UV to visible light range [11]. This red shift in the doped TiO_2 was attributed to the charge-transfer transition between the d-orbital electrons of the dopant and conduction band (CB) or valence band (VB) of TiO_2 [12]. Regarding to the non-metal doping, Umebayashi et al. [13–15] have succeeded to synthesize S-doped TiO_2, which was used as an efficient visible-light-induced photocatalyst for photocatalytic degradation of methylene blue. They found substitution of lattice oxygen in TiO_2 by sulfur anion. Ohno et al. [16–18] found that S atoms could be incorporated as cations and replaces lattice Ti in the TiO_2. Zhao et al. [19] and Majima and co-workers [20] reported that doping of TiO_2 with sulfur can also reduce its band gap and shift its optical response to the visible-light region.

In order to further improve the photocatalytic activity, codoping of TiO_2 with binary non-metals [21–24], metal and non-metal [25–28], metal and metal [29,30] and other semiconductors [31] has been explored. In this respect, codoping of TiO_2 with rare-earth transition metal and non-metallic element has aroused great attention [32,33]. Several studies demonstrated that the codoping with transition metal and nonmetallic element could effectively modify the electronic structures of TiO_2 and shift its absorption edge to lower energies [34,35].

The codoping of TiO_2 with transition metal and nonmetal elements has some positive aspects: narrowing the band gap and inhibition of charge recombination of the photo-generated electron-hole pairs. In the previous study, it was reported that TiO_2 absorption spectrum can be extended to the visible light region by incorporating Cr as metal an S as nonmetal into the TiO_2 crystallite [36]. The same results were reported for In- and S-codoped TiO_2 [37]. Ag and S co-doped TiO_2 degraded acetaldehyde ten times faster in visible light and 3 times faster in UV light illuminations compared to that of undoped TiO_2 [38]. It was also reported that La and N codoped TiO_2 nanoparticles showed a superior photocatalytic activity on degradation of methyl orange under visible light irradiation compared to the sole N-doped or La-doped TiO_2 [39].

The aim of the current study, which to best of our knowledge is done for the first time, is to study the synergetic effect of codoping of Mo and S on the photocatalytic activity of TiO_2 photocatalyst. The physico-chemical characteristic of the prepared catalysts were investigated by XRD, SEM, TEM, EDX, and UV-Vis DRS. Methyl orange (MO) was used as model organic pollutant to analyze photocatalytic performance of the prepared catalysts. Finally, it was

[a] Department of Chemistry, The University of Texas at El Paso, El Paso, Texas 79968, USA.
[b] Institute of Nanoscience and Nanotechnology, University of Kashan, Kashan, Iran.
[c] Department of Physical Chemistry, Faculty of Chemistry, University of Kashan, Kashan, Iran.
*Corresponding author; Tel +98 31 55912382; Fax +98 31 55912397; P.O. Box 87317-51167. Email: hamadani@kashanu.ac.ir (M. Hamadanian) & vahid_jabbari.azeri@yahoo.com (V. Jabbari).

found that the Mo,S-codoped TiO_2 shows a nanoscale size with strong light absorbance and high quantum efficiency and the 0.06Mo-0.05S/TiO_2 catalyst exhibited superior photocatalytic activity compared to the bare TiO_2 and sole Mo- or S-doped TiO_2 photocatalysts under UV and visible light irradiation.

2. Experimental

2.1. Chemicals

Ammonium heptamolibdate tetrahydrate ($(NH_4)_6Mo_7O_{24}.4H_2O$), thiourea, titanium(IV) isopropoxide, glacial acetic acid, ethanol, and nitric acid were purchased from Merck and were used without any further purification. Deionized water that was prepared by an ultra-pure water system type smart-2-pure made in TKA company of Germany was used throughout.

2.2. Synthesis of Mo and S doped TiO_2 Nanocatalysts

The typical synthesis procedure of pure TiO_2 nanoparticles has been described in our previous work [36]. Preparation procedure of S-doped TiO_2 nanoparticles was the same as for that of pure TiO_2, except the adding water contained the thiourea as source of S (corresponding to 0.05, 0.1, 0.15, 0.2, and 0.25 mol% with respect to TiO_2) [37].

The preparation of Mo,S codoped TiO_2 nanoparticles were was carried out via sol-gel method followed by photochemical reduction. In this regard, different amounts of $(NH_4)_6Mo_7.4H_2O$ as Mo precursor (corresponding to 0.03, 0.06 and 0.09 mol% with respect to TiO_2) was added to the S-doped TiO_2 suspended in 200 ml water, followed by purging by N_2 for 30 min to remove oxygen from the suspension. Afterwards, the pot was tightly capped and putted under UV irradiation for 12 h and Mo nanoclusters were formed and decorated over S-doped TiO_2 nanoparticles.

2.3. Assessment of Photocatalytic Performance of the Prepared Catalysts

The photocatalytic activity of the prepared catalysts was analyzed by MO degradation under UV and visible light irradiation. Each time, 0.1 gr photocatalyst was dispersed into 100 ml of 10 ppm MO aqueous solution with pH of around 2-3 in a quartz reactor (with a dimension of 12cm × 5cm, height and diameter, respectively). Two 400W Osram lamps were used as sources of visible and UV light, located 40 cm and 25 cm away from the reactor, respectively. Before light irradiation, the reaction system was stirred in dark for 30min to achieve absorption equilibrium.

2.4. Nanophotocatalyst Characterization

Crystalline phases of the prepared samples were analyzed by X-ray powder diffractometer (XRD, Bruker D8 Discover X-ray Diffractometer). The morphology was revealed by a transmission electron microscope (TEM, Hitachi H-7650) and scanning electron microscope (SEM, Hitachi S-4800) equipped with an energy dispersive X-ray detector (EDX). The diffused reflectance spectra (DRS) spectra of the samples were recorded by a Shimadzu 1800 spectrometer. UV-Vis absorption spectra of MO after the degradation tests were measured by UV-Vis spectrophotometer (Perkin Elmer Lambda2S, Germany). Raman spectra of the samples were collected from DXR™ Raman Microscope, Thermo Scientific.

3. Results and Discussions

3.1. Crystalline Structure

The X-ray diffraction patterns of the prepared nanocatalysts of 0.05% S/TiO2 with different amounts of Mo doping (0.03, 0.06, and 0.09%) (Fig. 1) and 0.06% Mo with different amounts of S doping (0.05, 1, 0.15, 0.2 and 0.25%) (Fig. 2) suggested the all samples possess high crystallinity with only anatase TiO_2 structure (2Θ= 25.2, 37.76, 48.02, 54.05, 55.03, 62.80, 68.85, 70.19, and 75.07) [36]. Furthermore, the XRD pattern did not show any metal-related phase (as metallic or metal oxide state) and it was concluded that metal ions are uniformly loaded over the TiO_2 surface.

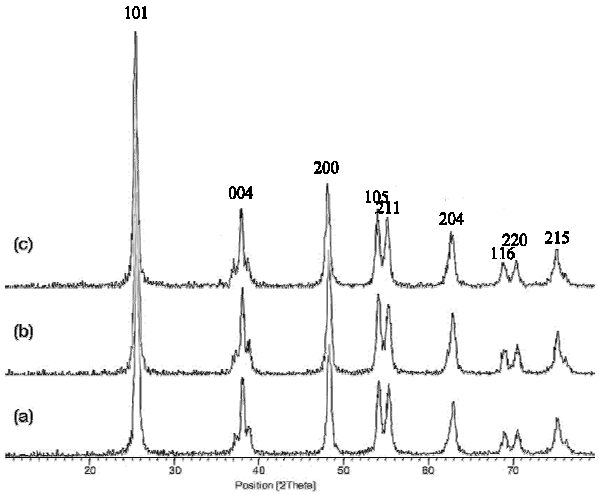

Fig. 1. XRD patterns of the 0.05% S/TiO_2 nanocatalysts with (a): 0.03, (b): 0.06, and (c): 0.09% Mo, prepared via photochemical deposition method. (A) represents anatase signals.

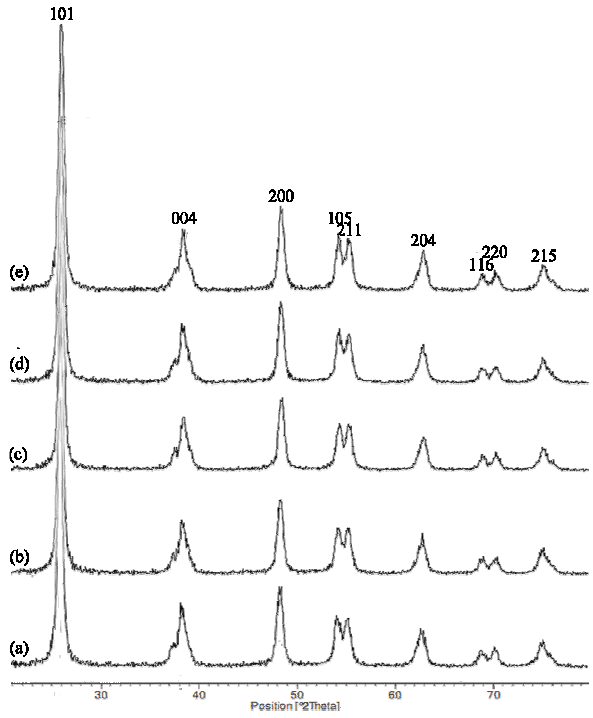

Fig. 2. XRD patterns of the 0.06% Mo/TiO_2 nanocatalysts with (a): 0.05, (b): 0.1, (c): 0.15, (d): 0.2, and (e): 0.25% S prepared via sol-gel method. (A) represents anatase signals.

Fig. 3 illustrates XRD patterns of pure TiO_2 and Mo(0.06),S(0.05)-codoped TiO_2 nanocatalysts. As shown, incorporation of metal and non-metal elements of Mo and S does not pose a significant change in crystalline structure of the TiO_2, and small shift in the positions of

the anatase peaks are observed in Mo(0.06),S(0.05)-codoped TiO_2 nanocatalysts compared to that of pure TiO_2.

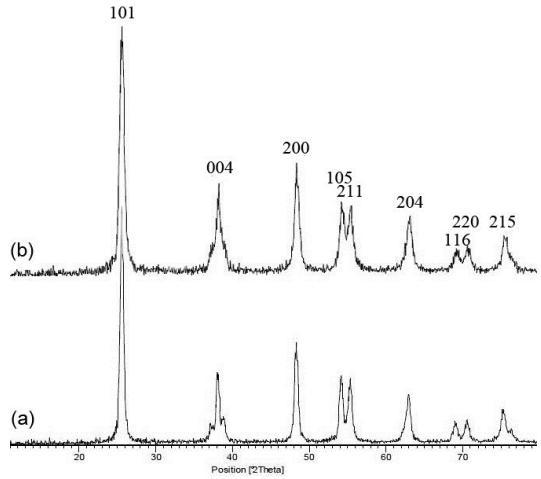

Fig. 3. XRD patterns of pure TiO_2 (a) and Mo(0.06),S(0.05)-codoped TiO_2 nanocatalysts (b). (A) represents anatase signals.

The average particle size (D, in nm) of the prepared catalysts was determined from XRD patterns according to the Scherrer's equation. The peak at 25.4◦ was used to calculate the average crystal size by Scherrer equation:

$D = K\lambda/\beta \cos\theta$ (1)

where *D* is the crystalline size, *λ* the wavelength of X-ray radiation (0.1541 nm), *K* the constant usually taken as 0.89, and β is the peak width at half-maximum height after subtraction of equipment broadening, 2θ = 25.4◦ for the anatase TiO_2. Average crystal size of pure TiO_2, S-doped TiO_2, Mo-doped TiO_2 and Mo,S-codoped TiO_2 found to be around 12–17 nm.

3.2. Morphological and Elemental Analysis

Fig. 4 shows SEM micrographs of the pure and Mo,S-codoped TiO_2 nanoparticles. The morphology of the nanoparticles was found to be uniform and slightly agglomerated spherical particles. Fig.4 also reveals that the doping of Mo and S does not pose any change in the morphology of the TiO_2 [35].

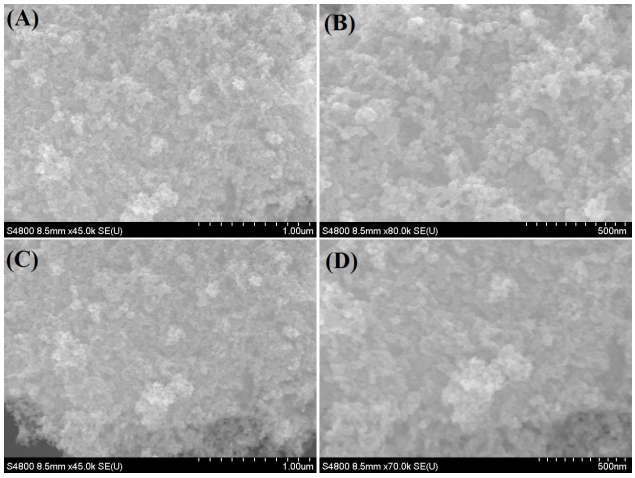

Fig. 4. SEM micrographs of pure TiO_2 (a,b) and Mo(0.06),S(0.05)-codoped TiO_2 (c,d).

Fig. 5 shows the corresponding EDX results of the Mo,S-codoped TiO_2 as the peaks of nonmetals element of S appears on the spectrum. The EDX spectrum further provides direct proof that Mo and S elements are successfully doped in TiO_2 as their characteristic peaks appears in the spectrum [37].

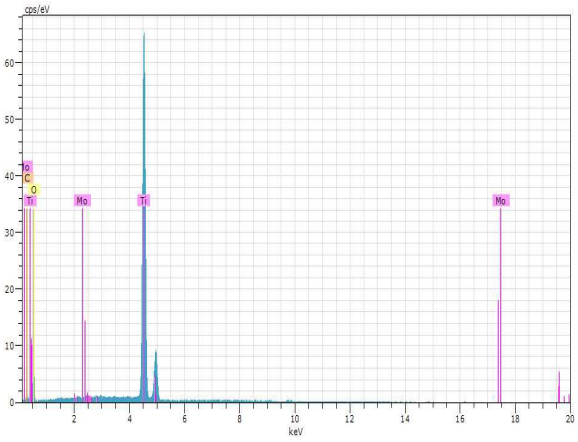

Fig. 5. EDX result of Mo(0.06),S(0.05)-codoped TiO_2 catalyst.

Size and morphology of prepared pure TiO_2 and Mo,S-codoped TiO_2 nanoparticles were also explored by TEM. Selected images are exhibited in Fig. 6. As it is obvious from Fig. 6, the nanoparticles are successfully synthesized which own spherical-shape morphology.

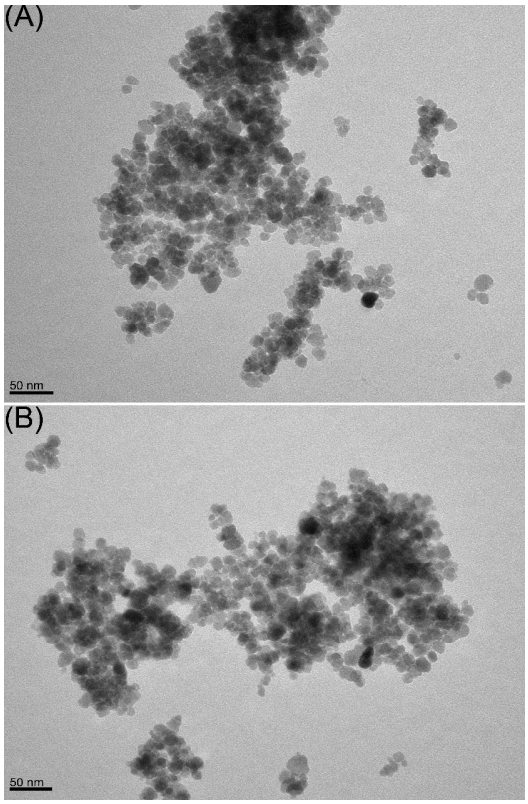

Fig. 6. TEM micrographs of pure TiO_2 (a) and Mo(0.06),S(0.05)-codoped TiO_2 (b).

3.3. Band Gap Analysis by DRS Spectroscopy

The DRS results of the prepared nanocatalysts are shown in Fig. 7. DRS results show a red shift in the absorption onset value in the case of Mo and S doped TiO_2, indicating decreases in band gap of the TiO_2 photocatalyst. Non-metal elements have been proven to be beneficial in reducing the band gap energy of TiO_2 through mixing their p-orbital with O2p-orbital, but the doping of transitional metals shift TiO_2 optical absorption edge from UV to visible light range without a prominent change in TiO_2 band gap [40-42]. The enhancement of absorbance in the UV–Vis region increases the number of photogenerated electrons and holes to participate in the photocatalytic reaction, which results in enhancement of the photocatalytic activity of TiO_2 [43].

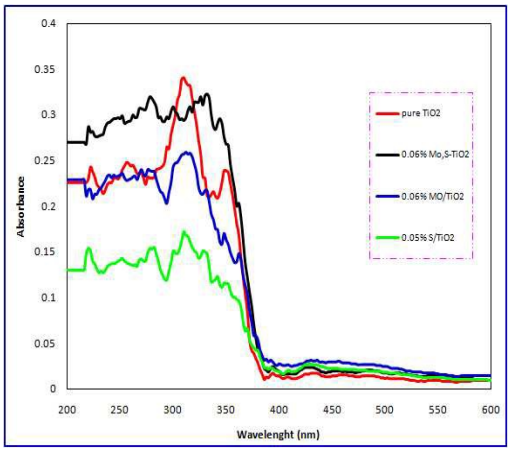

Fig. 7. UV-Vis DRS results of pure TiO_2, and Mo- and S-doped TiO_2 nanocatalysts.

3.4. Raman Analysis

In order to investigate chemical properties of the prepared nanocatalysts and effect of binary doping in chemical structure of TiO_2, Raman analysis was undertaken which the corresponding results are shown in Fig. 8. Anatase TiO_2 shows six peaks as follows: 144 cm^{-1} (E_g), 197 cm^{-1} (E_g), 399 cm^{-1} (B_{1g}), 513 cm^{-1} (A_{1g}), 519 cm^{-1} (B_{1g}) and 639 cm^{-1} (E_g), at which rutile phase has four bands at 143 cm^{-1} (B_{1g}), 447 cm^{-1} (E_g), 612 cm^{-1} (A_{1g}), and 826 cm^{-1} (B_{2g}) [44]. The findings related to Mo(0.06%),S(0.05%)-codoped TiO_2 shows identical signals of pure anatase TiO_2 with a slight chemical shift. In addition, intensity of the peaks at Mo(0.06%),S(0.05%)-codoped TiO_2 varies from that of pure TiO_2 which can be due to surface coverage of it by Mo nanoclusters [45].

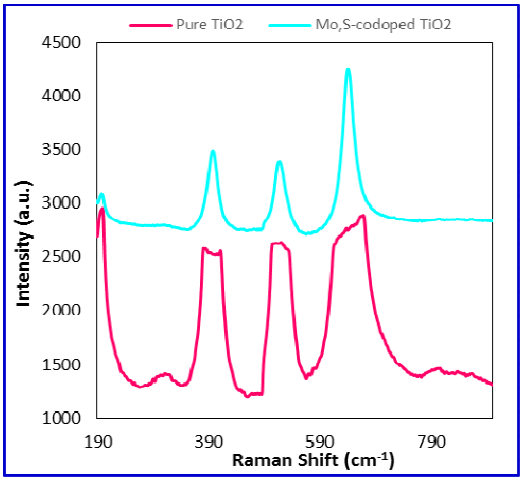

Fig. 8. Raman spectra of pure TiO_2, and Mo(0.06%),S(0.05%)-codoped TiO_2 nanocatalysts.

3.5. Photocatalytic Performance of the Prepared Nanocatalysts

Photocatalytic degradation of MO by undoped as well as Mo, and S-doped TiO_2 nanocatalysts under UV and visible light irradiation was evaluated. Fig. 9 and Table 1 show MO degradation by S/TiO_2 nanoparticles prepared by sol-gel method with different dose of S under UV and visible light irradiation.

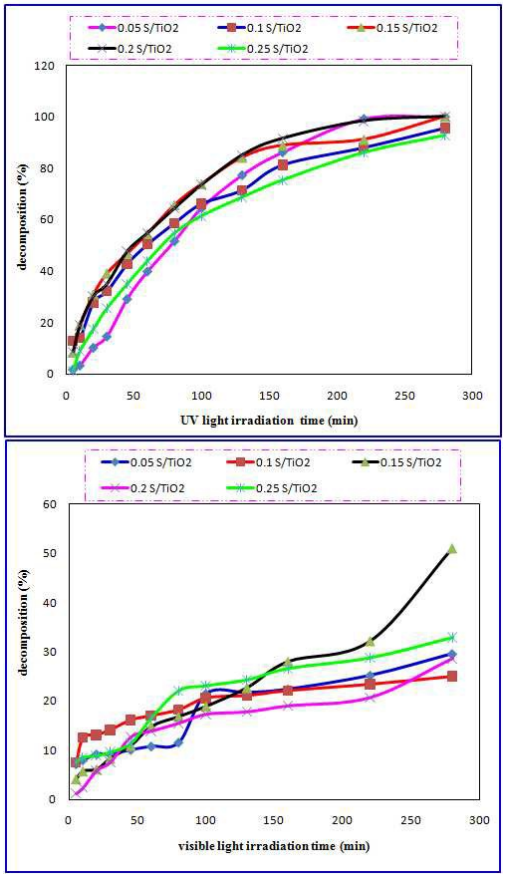

Fig. 9. The photocatalytic results of MO degradation using TiO_2 nanoparticles doped with different amounts of S under UV and visible light irradiation.

Table 1. The photocatalytic results of MO degradation using TiO_2 nanoparticles doped with different amounts of S under UV and visible light irradiation.

UV Light					
Elem. (%)	**0.05**	**0.10**	**0.15**	**0.20**	**0.25**
Time (min)					
5	1.6	12.7	8.3	8.6	1.3
10	3.2	13.9	19.1	18.8	8.9
20	10.1	27.8	30.9	30.1	17.4
30	14.5	32.1	39.1	34.9	25.5
45	29.1	42.7	46.8	47.6	34.9
60	39.8	50.3	54.5	54.7	43.9
80	51.6	58.6	65.7	64.3	54.7
100	64.5	66.1	73.8	73.4	61.4
130	77.3	71.4	84.1	85	68.6
160	86.2	81.2	88.8	91.5	75.3
220	99.2	87.9	91.1	98.3	86
280	100	95.5	100	100	92.7
Visible Light					
Elem. (%)	**0.05**	**0.10**	**0.15**	**0.20**	**0.25**
Time (min)					
5	7.2	7.5	4.1	1.2	7.6
10	8	12.5	5.7	2.4	8.5
20	8.9	13.1	6.1	5.9	8.9
30	9.2	14.1	8.3	7.6	9.6
45	10.1	16.1	10.9	12.7	11.4
60	10.8	17.0	14.8	13.9	16.6
80	11.6	18.2	16.8	15.5	22.1
100	21.5	20.6	18.9	17.3	23.1
130	21.7	21.1	22.7	17.8	24.3
160	22.4	29.1	28	19.0	26.6
220	25.2	23.4	32.2	20.7	28.8
280	29.6	25	51.1	28.6	32.9

Fig. 10 and Table 2 show degradation of MO under UV and visible light irradiation for Mo-doped TiO_2 nanoparticles with 0.05% S/TiO2. Fig. 11 shows degradation of MO under UV and visible light irradiation for Mo,S-codoped TiO_2 nanoparticles with 0.06% Mo and 0.05% S.

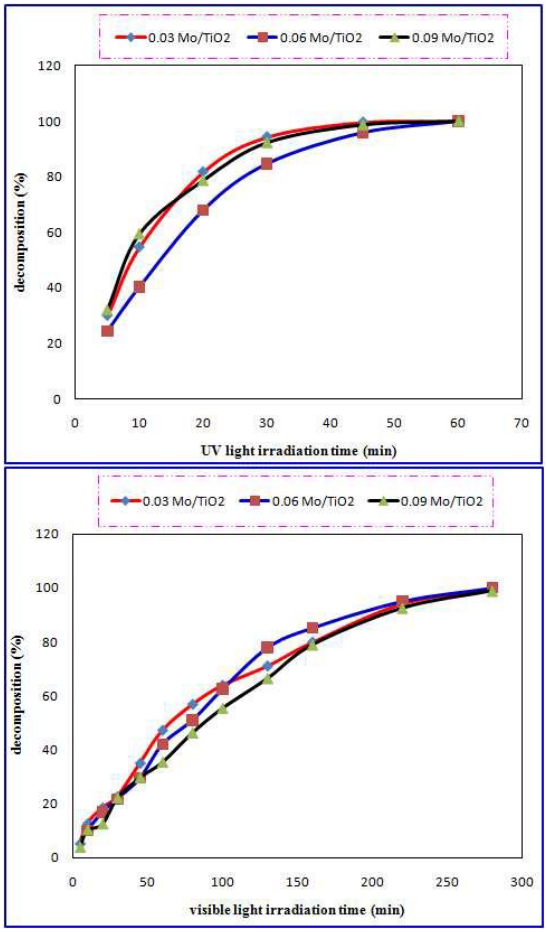

Fig. 10. The photocatalytic results of MO degradation using TiO_2 nanoparticles doped with 0.05% S and different amounts of Mo under UV and visible light irradiation.

Table 2. The photocatalytic results of MO degradation using Mo-doped TiO_2 nanoparticles with 0.05% S under UV and visible light irradiation.

UV Light			
Elem. (%)	**0.03**	**0.06**	**0.09**
Time (min)			
5	29.9	24.5	32.3
10	54.6	40.3	59.5
20	81.7	68	78.7
30	94.3	84.7	92.3
45	99.6	95.9	98.7
60	100	100	100
Visible Light			
Elem. (%)	**0.03**	**0.06**	**0.09**
Time (min)			
5	5.3	10.1	3.7
10	12.7	16.9	10.2
20	18.6	21.8	12.4
30	22.8	29.5	22.1
45	35.1	42.1	29.7
60	47.3	51	35.4
80	56.9	62.5	46.3
100	64	77.9	55.4
130	71.1	85.2	66.5
160	79.9	95.1	79

220	94.2	100	92.6
280	99.6	-	99

During the photocatalytic process, the absorption of photons by the photocatalyst leads to the excitation of electrons from the VB to the CB and generates electron–hole pairs. The electron in the conduction band is captured by oxygen molecules dissolved in the suspension and the hole in the VB can be captured by OH^- or H_2O species adsorbed on the surface of the catalyst, to produce the hydroxyl radical. Hydroxyl radicals then oxidize the pollutants. Thus, recombination of photogenerated electrons and holes is one of the most significant factors impacting the photoactivity of TiO_2 [43].

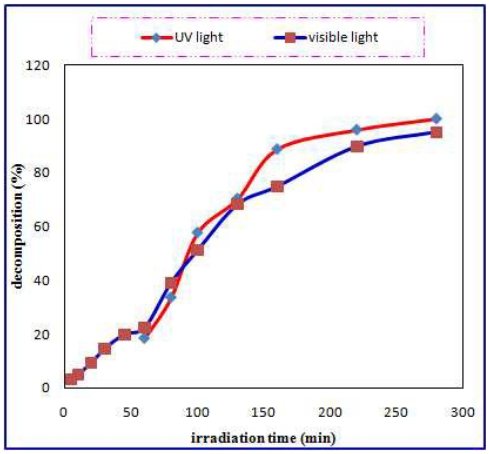

Fig. 11. The photocatalytic results of MO degradation using Mo,S-codoped TiO_2 nanoparticles with 0.05% S and 0.06% Mo.

Results exhibit that Mo,S-codoped TiO_2 nanoparticles prepared by photochemical method has higher activity than that of undoped TiO_2 or TiO_2 doped with either Mo or S. In particular, doping of TiO_2 by either Mo or S increases photocatalytic activity, but codoping of Mo and S enhances the photocatalytic activity with higher rate. The significantly higher photocatalytic performance of Mo,S-codoped TiO_2 may be due to the synergetic effect of the co-doping of S and Mo in TiO_2 nanoparticles. Presence of S reduces the band gap of TiO_2 and Mo nanoclusters located over the TiO_2 catalyst functions as electron scavenger (formation of Schottky barrier) and inhibit charge recombination of photogenerated electron-hole pairs at the surface of the catalyst as shown in Scheme 1 [46]. Overall, it is speculated that the higher photocatalytic activity of Mo,S-codoped TiO_2, is due to either one or combination of the following factors: (i) increased light absorption capability of Mo,S-codoped TiO_2 compared to undoped TiO_2 (ii) alleviation of the surface poison phenomenon; and (iii) reduction of the recombination rate of the photogenerated electron-hole pairs. Mo can act as both electron and hole trap to reduce the recombination rate and enhance the photocatalytic activity of TiO_2 [47].

In overall, we think that due to the excellent features deriving from synergetic effects of binary metal and non-metal doping, the newly developed Mo,S-codoped TiO_2 photocatalyst can be promising candidate for environmental applications such as air and water purification.

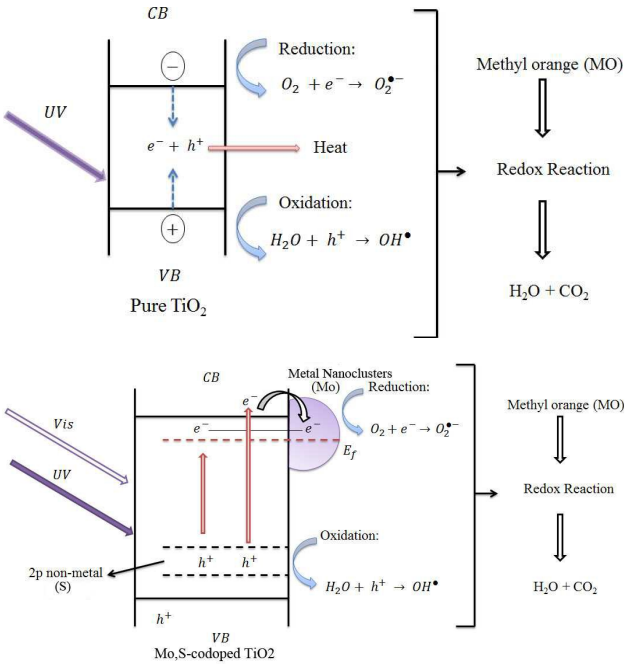

Scheme 1. Mechanism of degradation of MO by pure TiO_2 and Mo,S-codoped TiO_2 photocatalyst through. The scheme shows band gap reduction and formation of Schottky barrier in Mo,S-codoped TiO_2 photocatalyst compared to the pure TiO_2.

4. Conclusions

The sulfur and molybdenum codoped TiO_2 photocatalys of Mo,S-codoped TiO_2 were successfully prepared by modified sol–gel in conjunction with photochemical reduction method and the synthesized photocatalysts were used to degrade MO as model organic pollutant. XRD patterns showed high crystalline nature of the prepared catalysts at which only anatase phase was detected in all the undoped and doped samples. Morphological analyses performed by SEM and TEM showed relatively agglomerated spherical nanoparticles. EDX and DRS analyses further confirmed successful doping of Mo and S in TiO_2 and synthesis of Mo,S-codoped TiO_2. In general, our findings showed that codoping of TiO_2 with Mo and S led to less particle size, lower band gap values, red shift in light absorption threshold, and formation of Schottky barrier at the interface between TiO_2 and Mo nanoclusters. Photocatalytic activity of the samples was tested over degradation of MO as model organic pollutant and the findings showed that Mo,S-codoped TiO_2 nanoparticles have higher photocatalytic activity than undoped TiO_2 as well as sole Mo- or S-doped TiO_2 samples under UV and visible light, which this promotion in photocatalytic performance was ascribed to the synergetic effect of S and Mo. In conclusion, our results show Mo,S-codoped TiO_2 is a promising photocatalyst and can be a good candidate for various environmental applications.

Acknowledgment

We are grateful to Council of University of Kashan, Iran Nanotechnology Initiative Council and The University of Texas at El Paso (UTEP) for providing financial support. We also thank Dr. Maryam Zarei-Chaleshtori for helping us with SEM and XRD analyses, Dr. Peter Cooke from New Mexico State University (NMSU) for helping us with TEM analysis, Dr. Luis Echegoyen's lab for access to the Raman instrument, and the College of Engineering at UTEP for allowing access to their SEM and XRD instruments.

References

1 N. Zhang, M.-Q. Yang, S. Liu, Y. Sun, Y.-J. Xu, Chem. Rev. 2015, **115**, 10307.
2 M.-Q. Yang, N. Zhang, M. Pagliaro, Y.-J. Xu, Chem. Soc. Rev. 2014, **43**, 8240.
3 Y. Zhang, Z.R. Tang, X. Fu, Y.J. Xu, ACS Nano 2010, **4**, 7303.
4 X. Chen, S.S. Mao, Chem. Rev. 2007, **107**, 2891.
5 C. Han, M.-Q. Yang, N. Zhang, Y.-J. Xu, J. Mater. Chem. A, 2014, **2**, 19156.
6 N. Clifford, E. Palomares, K. Nazeeruddin, R. Thampi, M. Grtzel, J.R. Durrant, J. Am. Chem. Soc. 2004, **126**, 5670.
7 W. Zhao, C.C. Chen, X.Z. Li, J.C. Zhao, J. Phys. Chem. B 2002, **106**, 5022.
8 M. Jakob, H. Levanon, P.V. Kamat, Nano Lett. 2003, **3**, 353.
9 R. Asahi, T. Morikawa, T. Ohwaki, K. Aoki, Y. Taga, Science 2001, **293**, 269.
10 D.M. Chen, D. Yang, Q. Wang, Z.Y. Jiang, Ind. Eng. Chem. Res. 2006, **45**, 4110.
11 J.C.S. Wu, C.H. Chen, J. Photochem. Photobiol. A: Chem. 2004, **163**, 509.
12 M. Anpo, M. Takeuchi, J. Catal. 2003, **216**, 505.
13 T. Umebayashi, T. Yamaki, H. Itoh, K. Asai, Appl. Phys. Lett. 2002, **81**, 454.
14 T. Umebayashi, T. Yamaki, S. Tanala, K. Asai, Chem. Lett. 2003, **32**, 330.
15 T. Umebayashi, T. Yamaki, S. Yamamoto, A. Miyashita, S. Tanala, T. Sumita, K. Asai, J. Appl. Phys. 2003, **93**, 5156.
16 T. Ohno, T. Mitsui, M. Matsumura, Chem. Lett. 2003, **32**, 364.
17 T. Ohno, M. Akiyoshi, T. Umebayashi, K. Asai, T. Mitsui, M. Matsumura, Appl. Catal. A 2004, **265**, 115.
18 T. Ohno, Water Sci. Technol. 2004, **49**, 159.
19 W. Zhao, W. Ma, C. Chen, J. Zhao, Z. Shuai, J. Am. Chem. Soc. 2004, **126**, 4782.
20 T. Tachikawa, S. Tojo, K. Kawai, M. Endo, M. Fujitsuka, T. Ohno, K. Nishijima, Z. Miyamoto, T. Majima, J. Phys. Chem. B 2004, **108**, 19299.
21 D. Chen, Z. Jiang, J. Geng, Q. Wang, D. Yang, Ind. Eng. Chem. Res. 2007, **46**, 2741.
22 L. Lin, R.Y. Zheng, J.L. Xie, Y.X. Zhu, Y.C. Xie, Appl. Catal. B: Environ. 2007, **76**, 196.
23 X. Li, R. Xiong, G. Wei, Catal. Lett. 2008, **125**, 104.
24 F. Wei, L. Ni, P. Cui, J. Hazard. Mater. 2008, **156**, 135.
25 D.B. Hamal, K.J. Klabunde, J. Colloid Interf. Sci. 2007, **311**, 514.
26 K. Obata, H. Irie, K. Hashimoto, Chem. Phys. 2007, **339**, 124.
27 W. Pingxiao, T. Jianwen, D. Zhi, Mater. Chem. Phys. 2007, **103**, 264.
28 H. Huang, K. Liu, K. Chen, Y. Zhang, Y. Zhang, S. Wang, J. Phys. Chem. C 2014, **118**, 14379.
29 D.R. Zhang, Y.H. Kim, Y.S. Kang, J. Curr. Appl. Phys. 2006, **6**, 801.
30 R. Khan, S.W. Kim, T.-J. Kim, C.-M. Nam, Mater. Chem. Phys. 2008, **112**, 167.
31 X. Yang, L. Xu, X. Yu, Y. Guo, Catal. Commun. 2008, **9**, 913.
32 X. Huili, Z. Huisheng, X. Dongchang, Z. Tao, J. Wuhan, Univ. Technol. Mater. Sci. Ed. 2008, pp. 467–471.
33 C. Liu, X. Tang, C. Mo, Z. Qiang, J. Solid State Chem. 2008, **181**, 913.
34 M. Hamadanian, S. Karimzadeh, V. Jabbari, D. Villagrán, Materials Science in Semiconductor Processing, 2016, **41**, 168.
35 V. Jabbari, M. Hamadanian, A. Reisi-Vanani, P. Razi, S. Hoseinifard, D. Villagrán, RSC Adv., 2015, **5**, 78128.
36 M. Hamadanian, A. Sadeghi Sarabi, A. Mohammadi Mehra, V. Jabbari, Applied Surface Science 2011, **257**, 10639.
37 M. Hamadanian, A. Reisi-Vanani, P. Razi, S. Hoseinifard, V. Jabbari, Applied Surface Science 2013, **285**, 121.
38 D. B. Hamal, and K. J. Klabunde, Journal of Colloid and Interface Science 2007, **311**, 514.
39 H. Wei, W. Wu, N. Lun, F. Zhao, J. Mater. Sci. 2004, **39**, 1305.
40 L. Gomathi Devi, S. Girish Kumar, B. Narasimha Murthy, Nagaraju Kottam; Catalysis Communications 2009, **10**, 794.
41 R. Long, N. J. English, Phys. Rev. B 2011, **83**, 155209.
42 R. Long, N. J. English, Chem. Mater., 2010, **22**, 1616.
43 H. Huang, X. Li, J. Wang, F. Dong, P. K. Chu, T. Zhang, Y. Zhang, ACS Catal. 2015, **5**, 4094.
44 K. L. Frindell, M. H. Bartl, A. Popitsch and G. D. Stucky, Angew. Chem., Int. Ed., 2002, **41**, 959.
45 K. R. Zhu, M. S. Zhang, Q. Chen and Z. Yin, Phys. Lett. A, 2005, **340**, 220.
46 M. Hamadanian, M. Shamshiri, V. Jabbari, Applied Surface Science 2014, **317**, 302.
47 M. Hamadanian, V. Jabbari, M. Asad, M. Shamshiri, I. Mutlay, Journal of the Taiwan Institute of Chemical Engineers, 2013, **44**, 748.

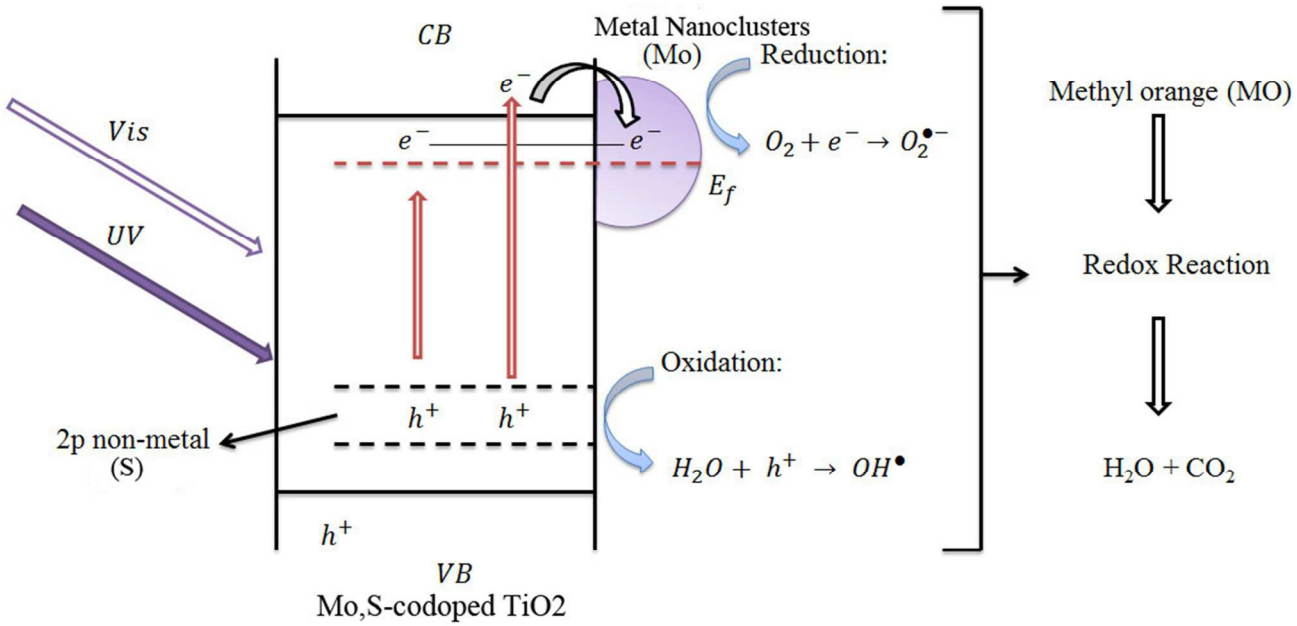

Mechanism of degradation of MO by pure TiO_2 and Mo,S-codoped TiO_2 photocatalyst through.